Title

Pink1 and Parkin regulate *Drosophila* intestinal stem cell proliferation during stress and aging.

Journal

The Journal of cell biology, 216(8)

ISSN

0021-9525

Authors

Koehler, Christopher L
Perkins, Guy A
Perkins, Guy A
et al.

Publication Date

2017-08-01

DOI

10.1083/jcb.201610036

Peer reviewed

Pink1 and Parkin regulate *Drosophila* intestinal stem cell proliferation during stress and aging

Christopher L. Koehler,[1,2,5] Guy A. Perkins,[3] Mark H. Ellisman,[3,4] and D. Leanne Jones[1,5,6,7]

[1]Laboratory of Genetics, Salk Institute for Biological Studies, La Jolla, CA
[2]Division of Biological Sciences, [3]National Center for Microscopy and Imaging Research, Center for Research in Biological Systems, and [4]Department of Neurosciences, University of California, San Diego, La Jolla, CA
[5]Molecular Biology Institute, [6]Department of Molecular, Cell, and Developmental Biology, and [7]Eli and Edythe Broad Center of Regenerative Medicine and Stem Cell Research, University of California, Los Angeles, Los Angeles, CA

Intestinal stem cells (ISCs) maintain the midgut epithelium in *Drosophila melanogaster*. Proper cellular turnover and tissue function rely on tightly regulated rates of ISC division and appropriate differentiation of daughter cells. However, aging and epithelial injury cause elevated ISC proliferation and decreased capacity for terminal differentiation of daughter enteroblasts (EBs). The mechanisms causing functional decline of stem cells with age remain elusive; however, recent findings suggest that stem cell metabolism plays an important role in the regulation of stem cell activity. Here, we investigate how alterations in mitochondrial homeostasis modulate stem cell behavior in vivo via RNA interference–mediated knockdown of factors involved in mitochondrial dynamics. ISC/EB-specific knockdown of the mitophagy-related genes Pink1 or Parkin suppresses the age-related loss of tissue homeostasis, despite dramatic changes in mitochondrial ultrastructure and mitochondrial damage in ISCs/EBs. Maintenance of tissue homeostasis upon reduction of Pink1 or Parkin appears to result from reduction of age- and stress-induced ISC proliferation, in part, through induction of ISC senescence. Our results indicate an uncoupling of cellular, tissue, and organismal aging through inhibition of ISC proliferation and provide insight into strategies used by stem cells to maintain tissue homeostasis despite severe damage to organelles.

Introduction

Tissue homeostasis in many adult metazoans is maintained via the activity of resident somatic stem cells. Through asymmetric, mitotic divisions, adult stem cells can self-renew to maintain the stem cell population and, simultaneously, give rise to daughter cells that can differentiate along a given lineage to replace lost or damaged cells. The long-term regenerative capacity of a tissue, therefore, relies heavily on the careful balance between stem cell self-renewal and the initiation of differentiation. Deregulation of stem cell function can lead to altered organ function that is detrimental to overall organismal health and life span (Jones and Rando, 2011).

Intestinal stem cells (ISCs) maintain the midgut epithelium in *Drosophila melanogaster* in a manner similar to their mammalian counterparts. Genetic tractability, a simple cell lineage, and conserved pathways that regulate ISC behavior combine to make the *Drosophila* midgut epithelium a powerful model system for the study of stem cell regulation and tissue homeostasis. Regional differences exist along the length of the midgut, although ISCs are involved in maintaining homeostasis throughout (Buchon et al., 2013; Marianes and Spradling, 2013). The ISCs of the posterior midgut reside adjacent to the basement membrane and undergo asymmetric division to maintain turnover of differentiated epithelial cells (Micchelli and Perrimon, 2006; Ohlstein and Spradling, 2006) or symmetric division to increase ISC numbers in response to nutritional cues (O'Brien et al., 2011). Asymmetric ISC division leads to generation of a new stem cell and a daughter cell, called an enteroblast (EB). Delta/Notch signaling between the ISC and EB dictates whether an EB will differentiate into an absorptive enterocyte (EC) or a secretory enteroendocrine cell (Ohlstein and Spradling, 2007; Maeda et al., 2008; Liu et al., 2010; Takashima et al., 2011), though data have indicated that enteroendocrine cells can also derive directly from ISCs (Biteau and Jasper, 2014; Guo and Ohlstein, 2015; Zeng and Hou, 2015).

Under normal, homeostatic conditions, the *Drosophila* midgut epithelium undergoes slow turnover (Micchelli and Perrimon, 2006; Ohlstein and Spradling, 2006), yet ISCs respond to several intrinsic and extrinsic stimuli that regulate proliferation (Amcheslavsky et al., 2009, 2011, 2014; Buchon et al.,

Correspondence to D. Leanne Jones: leannejones@ucla.edu

Abbreviations used: EB, enteroblast; EC, enterocyte; *esg* F/O, *esg*-mediated "flip out"; DHE, dihydroethidium; H2AvD, phospho–histone 2A variant D; ISC, intestinal stem cell; OMM, outer mitochondrial membrane; ROS, reactive oxygen species; SA–β-gal, senescence-associated β-galactosidase; STED, stimulation emission depletion; TEM, transmission EM.

The Rockefeller University Press
J. Cell Biol. Vol. 216 No. 8 2315–2327
https://doi.org/10.1083/jcb.201610036

2009a,b; Jiang and Edgar, 2009; Jiang et al., 2009; Lee, 2009; Biteau and Jasper, 2011; Li et al., 2013; Myant et al., 2013; Tian and Jiang, 2014). Importantly, ISC proliferation rates increase significantly in response to chemically induced damage or pathogenic bacterial infection. Although adaptive ISC divisions can maintain tissue homeostasis through the replenishment of lost or damaged cells, uncontrolled ISC division and altered differentiation programs can lead to loss of tissue function.

In the *Drosophila* midgut, aging results in the consistent manifestation of several ISC-related phenotypes, including an increase in ISC proliferation and a block in terminal differentiation of ISC progeny, as reflected by the accumulation of polyploid cells that express the ISC/EB marker Escargot (Esg). Consequently, this leads to alterations in localization of cell–cell junctional complexes, loss of the typical apical–basal organization of the epithelial monolayer, and a decline in intestinal barrier function (Biteau et al., 2010; Rera et al., 2011; Resnik-Docampo et al., 2017).

The ISCs are relatively long-lived cells with very few mitochondria (Fig. 1, A–C). Throughout the lifetime of a fly, the ISC must give rise to numerous differentiated cells, which requires extensive mitochondrial biogenesis to expand the mitochondrial mass to cope with increased energy demands. We recently demonstrated that ISC/EB–specific overexpression of *spargel (srl*), the *Drosophila* homologue of *PGC1α*, a master regulator of mitochondrial biogenesis, delays age-related changes to ISCs and the loss of intestinal homeostasis, leading to a dramatic increase in life span in both sexes (Rera et al., 2011). This suggested that mitochondrial metabolism is important in the regulation of ISC behavior, midgut homeostasis, and longevity; however, little is known about the role mitochondrial quality control plays in regulating stem cell function under homeostatic conditions, in response to damage, or with age.

We hypothesized ISCs would have a stringent mechanism for the removal of damaged mitochondria to avoid passage of damaged mitochondria or mitochondrial DNA mutations to differentiating daughter cells. Isolation and degradation of damaged mitochondria via selective autophagy (mitophagy) relies largely on two genes associated with autosomal-recessive juvenile parkinsonism: *parkin*, which encodes an E3 ubiquitin ligase, and *pink1* (phosphatase and tensin homologue-induced putative kinase 1), which encodes a mitochondria-targeted serine/threonine kinase. In *Drosophila*, both *pink1* and *parkin* mutants exhibit male sterility, loss of normal mitochondrial morphology, and muscle degeneration (Greene et al., 2003; Clark et al., 2006). Pink1 acts upstream of Parkin and is stabilized on the outer mitochondrial membrane (OMM) of mitochondria with collapsed membrane potentials (depolarized mitochondria). Stabilization of Pink1 on the OMM leads to the recruitment of Parkin, which, in turn, ubiquitinates several proteins on the OMM. Ubiquitinated proteins can be recognized by Ref(2)P, the *Drosophila* homologue of p62. Acting as an adaptor, Ref(2)P links the ubiquitinated cargo to the lipidated form of Atg8 (the *Drosophila* homologue of LC3) on a phagophore, ultimately leading to mitophagic degradation (Springer and Kahle, 2011; Youle and Narendra, 2011; Zhu et al., 2013; Wei et al., 2015). However, mitochondrial quality control is also achieved through constant remodeling of the mitochondrial network through fission and fusion (Poole et al., 2008, 2010; Twig et al., 2008; Yang et al., 2008; Kashatus et al., 2011; reviewed in Benard and Rossignol, 2008; Yang et al., 2008; Westermann, 2012). To identify mechanisms used by ISCs to maintain a healthy pool of mitochondria, we conducted an RNAi screen to deplete factors required for mitochondrial dynamics and examined the effects on the mitochondria, stem cell function, tissue homeostasis, and longevity. This approach revealed that depletion of Pink1 and Parkin in ISCs results in changes in ISC behavior, consistent with the onset of senescence.

Results and discussion

ISC/EB–specific knockdown of Pink1 or Parkin alters mitochondrial morphology and density

To determine whether genes involved in mitochondrial dynamics (fission, fusion, movement, and turnover) play a role in ISC function, we used the ISC/EB–specific, RU486-inducible *5961-Gal4^{GeneSwitch}* (*5961^{GS}*) "driver" to direct expression of *UAS*-RNAi lines in ISCs/EBs in the adult midgut (see Materials and methods for specific RNAi lines tested). Use of the drug-inducible system permits comparison of genetically identical individuals that are either expressing (+RU486) or not expressing (EtOH/−RU486) the transgene of interest. Overexpression of *srl* led to a decrease in intestinal dysplasia, as previously reported (Rera et al., 2011). However, in contrast to our expectations, RNAi-mediated depletion of Pink1 or Parkin resulted in a drastic improvement in intestinal homeostasis in aged flies. Manipulation of other factors tested had no significant effect on ISC maintenance or tissue homeostasis during the time points assayed (10, 30, and 50 d post-eclosion).

Mutations in the mitochondrial-associated proteins Pink1 and Parkin are among the causative factors in familial forms of Parkinson's disease (Henchcliffe and Beal, 2008). In *Drosophila*, loss-of-function mutations in *pink1* or *parkin* result in abnormal wing posture, along with several mitochondrial phenotypes, including defects in mitochondrial function, cristae morphology, and flight muscle mitochondrial morphology (Clark et al., 2006; Park et al., 2006; Deng et al., 2008). Alternatively, ubiquitous overexpression of Parkin limits the age-associated accumulation of polyubiquitin aggregates in the flight muscle (Rana et al., 2013). To verify the efficacy of Pink1 and Parkin RNAi lines, we crossed control RNAi (*UAS-mCherry^{RNAi}*), Pink1 RNAi (*UAS-pink1^{RNAi}*), or Parkin RNAi (*UAS-parkin^{RNAi}*) lines with the ubiquitous *Da-Gal4^{GeneSwitch}* driver (Fig. S1). Similar to *pink1* and *parkin* mutants, ubiquitous expression of Pink1 RNAi or Parkin RNAi resulted in abnormal flight muscle mitochondrial morphology (Fig. S1, A–C), mobility defects (Fig. S1, D–F), accumulation of polyubiquitin aggregates (Fig. S1, G–I and G′–I′), and abnormal wing posture (Fig. S1, J and K).

Because the flight muscle mitochondria of *pink1* and *parkin* mutants demonstrated abnormal cristae morphology, we sought to determine if RNAi-mediated depletion of Pink1 or Parkin showed similar mitochondrial phenotypes in ISCs. Therefore, we used transmission EM (TEM) to examine ISCs in posterior midguts from young (day 10) and old (day 55) flies (Fig. 1, A–F). Similar to previous TEM studies, progenitor cells were identified by basal localization within the midgut epithelium, contact with basement membrane, and a lack of cell–cell contacts with neighboring ECs (Han et al., 2015). In young flies, *pink1^{RNAi}* and *parkin^{RNAi}* caused altered cristae structure and increased electron density in the mitochondrial matrix (Fig. 1, A′–C′). In aged controls, the mitochondria in ISCs have a slightly varied morphology, when compared with

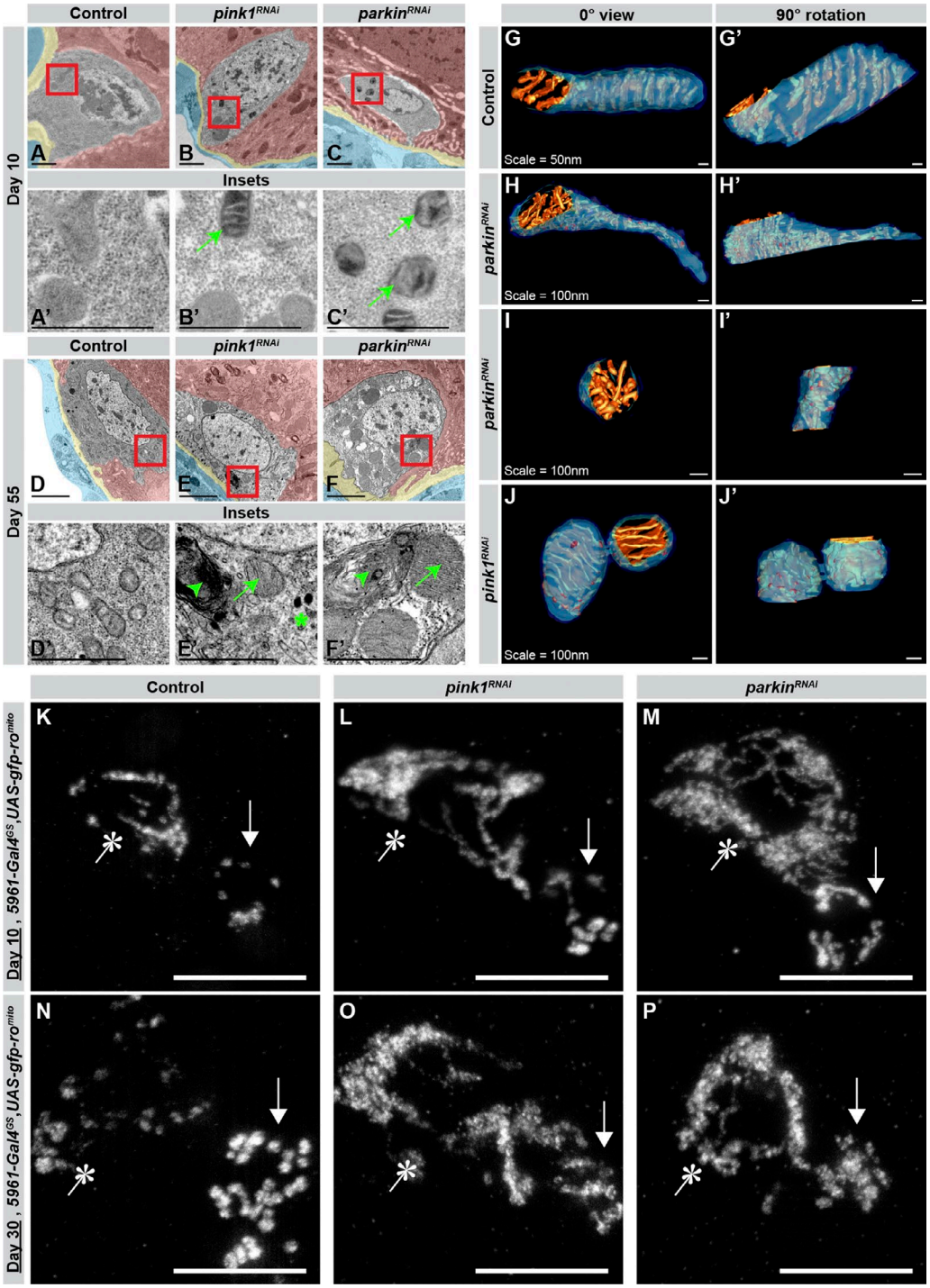

Figure 1. **ISC/EB–specific knockdown of Pink1 or Parkin alters mitochondrial morphology and density.** (A–F) Transmission electron micrographs of midgut progenitor cells in the posterior midgut of 10- or 55-d-old control, *Su(H)LacZ;esg-gfp,5961-Gal4^{GS}/+;UAS-mCherry^{RNAi}/+* (A and D, *n* = 4 and 10, respectively), Pink1 knockdown, *Su(H)LacZ;esg-gfp,5961-Gal4^{GS}/UAS-pink1^{RNAi}* (B and E, *n* = 3 and 6, respectively), or Parkin knockdown, *Su(H)LacZ;esg-gfp,5961-Gal4^{GS}/UAS-parkin^{RNAi}* (C and F, *n* = 3 and 5, respectively) adult flies. Visceral muscle (blue), basement membrane (yellow), and enterocytes (red) are labeled via pseudocolor. Bars, 1 µm. (A′–F′) Magnified regions outlined in A–F. Bars: (A′–C′) 1 µm; (D′–F′) 0.5 µm. Arrows indicate swollen or condensed mitochondria, arrowheads show multilamellar bodies (MLBs), and an asterisk denotes electron-dense granule accumulation. (G–J′) Reconstructed, segmented, and surface-rendered mitochondria from electron tomography of midgut progenitors in 55-d-old control, Pink1 knockdown, or Parkin knockdown posterior midguts (*n* = 4, 3, and 4, respectively). Outer mitochondrial membrane (OMM; dark blue), inner boundary membrane (IBM; light blue), and cristae (orange) are shown; the intersections of cristae with the IBM represent cristae junctions. (K–P) Stimulation emission depletion (STED) microscopy images of mitochondria in the ISCs/EBs from 10- (K–M) or 30-d-old (N–P) flies. *UAS-gfp-ro^{mito}* was used to label ISC/EB mitochondria and was visualized via immunofluorescent staining for GFP (see Materials and methods). Arrows point to ISCs, and asterisks indicate EBs. Bars, 5 µm.

young controls (Fig. 1 D′); however, knockdown of Pink1 or Parkin in aged samples resulted in significantly greater numbers of abnormal mitochondria, including swollen mitochondria with altered cristae shape, accumulation of multilamellar bodies, and the appearance of electron-dense granules (Fig. 1, E′ and F′; and Fig. S1, L, M, and N–N′′). Importantly, the alterations in mitochondrial morphology were restricted to the progenitors, as mitochondria in adjacent ECs exhibited wild-type morphology (Fig. S1, O and P). In contrast to enhanced tissue homeostasis observed upon ISC/EB–specific expression of Pink1 RNAi, the expression of Pink1 RNAi in the enterocytes via *5966-Gal4*^{GeneSwitch} led to loss of the epithelial monolayer and increased misexpression of the progenitor cell marker Escargot (Fig. S2, A–D). These data indicate that perdurance of RNAi expression into the differentiated cells of the midgut is not responsible for the observed phenotypes.

Several studies have demonstrated a relationship between mitochondrial ultrastructure and energetic state of the mitochondria (Hackenbrock, 1966; Benard and Rossignol, 2008). Specifically, mitochondria tend to exist in two major forms in vivo: orthodox and condensed. Larger matrix volumes and inner boundary membranes that are closely opposed to the outer mitochondrial membrane are characteristics of orthodox mitochondria, which correlate with low respiratory activity. Conversely, in periods of high respiratory activity, a mitochondrion can adopt the condensed configuration, in which the matrix volume is drastically decreased and the cristae become enlarged and often irregular with expanded cristae junctions (Hackenbrock, 1966). We conducted detailed, 3D electron tomographic reconstructions to ascertain whether the observed changes in mitochondrial morphology upon knockdown of Pink1 or Parkin represented an orthodox to condensed transition (Fig. 1, G–J and G′–J′). In unperturbed ISCs, the mitochondria tended to adopt an orthodox morphology, indicating that mitochondria of normal ISCs had low respiratory output (Fig. 1, G and G′). Conversely, many mitochondria within Pink1- or Parkin-depleted progenitor cells adopted an ultracondensed structure with enlarged intracristal space accompanied by reduced matrix volume (Fig. 1, H–J and H′–J′). Therefore, it appears that ISC/EB–specific reduction of the mitophagy-associated proteins Pink1 or Parkin causes changes in mitochondria that are typically associated with higher respiratory output. We performed several assays, including live imaging with the potentiometric dyes tetramethylrhodamine ethyl ester and MitoTracker red, in an attempt to determine whether intestinal progenitor cell mitochondria did, in fact, have higher respiratory outputs; however, technical limitations rendered the results inconclusive.

Proper function of Pink1 and Parkin is essential for the efficient elimination of damaged mitochondria via mitophagy; therefore, in addition to altered mitochondrial substructure, loss of Pink1 or Parkin function could affect mitochondrial abundance and network formation. We examined the effect of Pink1/Parkin depletion on the mitochondrial network of ISCs/EBs via stimulated emission depletion (STED) microscopy. The mitochondrial networks appeared much more fused upon progenitor-specific depletion of Pink1 or Parkin (Fig. 1, L, M, O, and P) in comparison to controls (Fig. 1, K and N). Because Pink1/Parkin activity results in Mfn ubiquitination and degradation, the increasingly fused mitochondrial networks may be the result of decreased Mfn turnover. In contrast, aging resulted in the accumulation of more punctate mitochondria in the ISCs of control flies, but not in ISCs depleted of Pink1 or Parkin (Fig. 1, compare K with N–P, arrows). Collectively, these data demonstrate that progenitor-specific RNAi-mediated depletion of Pink1 or Parkin disrupts normal mitochondrial structure in ISCs/EBs.

Progenitor-specific knockdown of Pink1 or Parkin delays tissue level aging phenotypes in the posterior midgut

Recent studies indicate that changes in metabolism-associated factors such as altered nutrient availability, mitochondrial abundance, or electron transport chain function can impact ISC behavior and tissue homeostasis in the *Drosophila* midgut (O'Brien et al., 2011; Rera et al., 2011; Wang et al., 2011; Hur et al., 2013). Given the influence of Pink1 and Parkin on cellular metabolism via their roles in mitophagy, we investigated the effect of progenitor-specific loss of Pink1 or Parkin on tissue homeostasis in the posterior midgut. To assay tissue homeostasis, we performed several assays for phenotypes that consistently manifest as a consequence of aging in the fly including: increased ISC mitoses (pHH3$^+$ cells), expanded expression of the ISC/EB marker Esg, and loss of the epithelial monolayer.

To test whether midgut homeostasis is affected by loss of Pink1 or Parkin in the progenitor cells, we used an inducible *esg*-mediated "flip-out" (*esg* F/O) system (Jiang et al., 2009) to generate clones in which all ISCs/EBs and their progeny express a UAS-RNAi construct of interest, as well as UAS-*gfp*. After rearing flies at 18°C, transgene expression was induced 1 to 2 d after eclosion by culturing flies at 29°C. Clonal expansion was assayed after 7 or 25 d (Fig. 2, A–C and A′–C′). Interestingly, although the number of cells per clone is the same across all groups after 7 d of transgene induction (Fig. 2 D, left), loss of Pink1 or Parkin significantly reduced the mean number of cells per clone after 25 d (Fig. 2 D, right). Furthermore, loss of Pink1 or Parkin resulted in significantly smaller clonal areas at 7 and 25 d after clone induction (Fig. 2 E).

As the *esg* F/O system is engineered to label the progenitor cells and their progeny, we expected many of the flip-out clones to include large, differentiated ECs under normal conditions. Indeed, in the control groups, the mean area of each clone, which included large, polyploid ECs (Fig. 2, A and A′), increases over time (Fig. 2 E). However, clones expressing either *pink1*^{RNAi} or *parkin*^{RNAi} demonstrated a noticeable lack of ECs, even 25 d after clone induction (Fig. 2, B, B′, C, and C′). The lack of differentiated cells and smaller clone sizes could be the result of either a lack of ISC mitotic divisions or induction of cell death upon differentiation in Pink1/Parkin knockdown clones. To test the first possibility, we measured ISC proliferation in guts from *esg* F/O flies 7 or 25 d after induction of transgene expression. We found that basal proliferation rates of ISCs in the young, male midgut were low enough as to be undetectable by pHH3 staining in either control (*mCherry*^{RNAi}) or test (*pink1*^{RNAi} or *parkin*^{RNAi}) groups (Fig. 2 F), but an increase in ISC proliferation was detected in guts from older control males. Interestingly, the previously described age-associated increase in ISC mitoses was almost completely abrogated in the Pink1/Parkin knockdowns (Fig. 2 F). These data indicate that the reduced clone size and clone cell numbers observed upon RNAi-mediated knockdown of Pink1 or Parkin are caused by a decrease in ISC proliferation rather than the increase normally observed as a consequence of aging.

The *esg* F/O system induces expression of transgenes in the midgut progenitor cells, as well as any resulting progeny; therefore, the effects of Pink1/Parkin loss on ISC behavior could

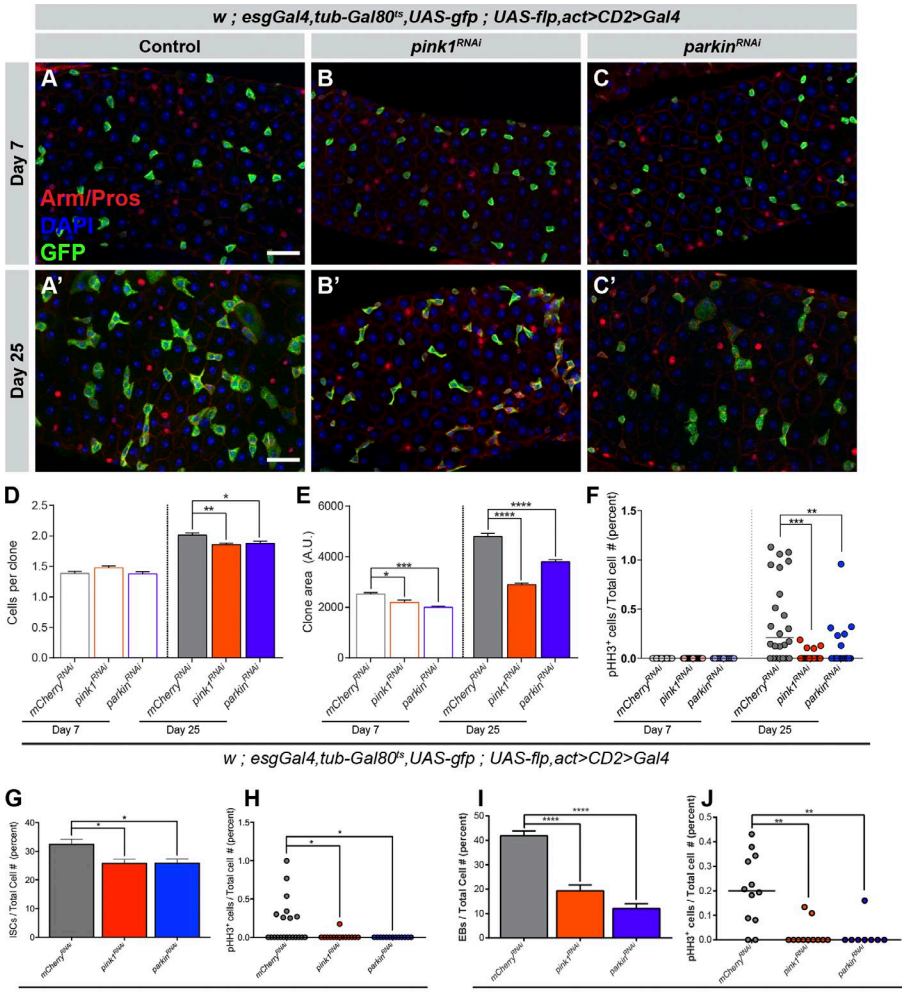

Figure 2. **Progenitor-specific knockdown of Pink1 or Parkin delays tissue level aging phenotypes in the posterior midgut.** (A–C′) Representative immunofluorescence images of the posterior midgut of 7- or 25-d-old control (*esg-Gal4, tub-GAL80^{ts}, UAS-gfp/+; UAS-flp, act*>CD2>Gal4/UAS-*mCherry^{RNAi}*), Pink1 knockdown (*esg-Gal4, tub-GAL80^{ts}, UAS-gfp/UAS-pink1^{RNAi}; UAS-flp, act*>CD2>Gal4/+), or Parkin knockdown (*esg-Gal4, tub-GAL80^{ts}, UAS-gfp/UAS-parkin^{RNAi}; UAS-flp, act*>CD2>Gal4/+) flies aged at 29°C. Armadillo (Arm; membrane) was used to delineate cell boundaries and assay epithelial morphology. Prospero (Pros; nuclear) marks enteroendocrine cells. Bars, 20 µm. (D) Quantification of the number of cells comprising each *esg F/O* clone from A–C′. (E) Groups of contiguous GFP-positive cells were classified as individual *esg F/O* clones. The mean area of all clones per treatment group is represented. For D–E, $n_{guts/clones}$ = 6/524, 9/923, 5/343, 13/1,713, 13/2,216, and 10/1,508. (F) Quantification of actively dividing (pHH3$^+$ cells) from A–C′ (n_{guts} = 18, 27, 15, 24, 21, and 22). (G and H) Quantification of the proportion of ISCs in the posterior midgut (G) or mitotic ISCs (H) upon ISC-specific knockdown of mCherry, Pink1, or Parkin in 25-d-old-flies (n_{guts} = 21, 14, and 13). (I and J) Quantification of the proportion of EBs in the posterior midgut (I) or mitotic ISCs (J) upon EB-specific knockdown of mCherry, Pink1, or Parkin (n_{guts} = 12, 11, and 8). Datasets D, E, G, and I represent means ± SEM and were analyzed using one-way ANOVA followed by a Dunnett's post test to determine significant differences in means. For datasets F, H, and J, each age group was analyzed independently using a Kruskal–Wallis test for nonparametric data followed by a Dunn's post test for multiple comparisons to determine significantly different median values. *, P < 0.05; **, P < 0.01; ***, P < 0.001; ****, P < 0.0001.

result from non–cell autonomous activity caused by knockdown in differentiated progenitor cells. To determine if depletion of Pink1 or Parkin specifically in ISCs or EBs was sufficient to reduce ISC proliferation and gut turnover, we directed expression of *UAS-pink1^{RNAi}* or *UAS-parkin^{RNAi}* to ISCs, EBs, or both cell types. Using an *esg-Gal4* driver under the control of the temperature-sensitive *tub-Gal80^{ts}* transgene (referred to as *esg^{ts}*), expression was restricted to ISCs/EBs of the adult midgut for 25 d by shifting the flies to 29°C. In contrast to controls, the previously reported, age-associated misexpression of *esg* was significantly reduced upon Pink1 or Parkin depletion (Fig. S2, E–E′′ and F). Furthermore, ISC-specific expression of *pink1* or *parkin* RNAi along with a *UAS-2X-yfp* reporter (ISC-Gal4; Wang et al., 2014) also revealed an abrogation in the normal increase in ISC number 25 d after induction of the RNAi transgenes (Fig. 2 G and Fig. S2, G–G′′). In addition, ISC-specific depletion of Pink1 or Parkin was sufficient to cause a significant reduction in ISC proliferation (Fig. 2 H). Similarly, specific knockdown of Pink1 or Parkin in EBs using a temperature-sensitive version of the *Su(H)Gal4* driver (EB-Gal4; Zeng et al., 2010) resulted in fewer EBs 25 d after induction of the RNAi (Fig. 2 I and Fig. S2, H–H′′). Interestingly, EB-directed knockdown of Pink1 or Parkin also resulted in a non–cell-autonomous reduction in ISC proliferation (Fig. 2 J). These data indicate that either Pink1 or Parkin can act independently in ISCs or EBs to inhibit the age-associated increase in ISC proliferation.

Because increased ISC proliferation and *esg* misexpression are intimately linked with age, it was important to determine whether the different fly lines being compared have similar life spans to avoid misinterpretation of the data based on different rates of aging. We preformed life span assays using the *5961^{GeneSwitch}* (*5961^{GS}*) driver; this allowed drug inducible expression of the RNAi transgenes to avoid any differences that could be attributed to different genetic backgrounds. In addition, we crossed the *5961^{GS}* driver to *UAS-mCherry^{RNAi}* to validate its use as a control in other assays. In all cases, our data indicated that progenitor specific knockdown of mCherry (control), Pink1, or Parkin had no effect on life span (Fig. S3, A–C).

Progenitor-specific depletion of Pink1 or Parkin limits the normal proliferative response to stress in the young midgut

Our findings indicate that progenitor-specific loss of Pink1 or Parkin results in the suppression of ISC proliferation and *esg* misexpression with age, which accompany severe alterations in mitochondrial morphology. However, it was not apparent whether suppression of ISC proliferation was restricted to aging or whether loss of Pink1/Parkin would suppress induction of

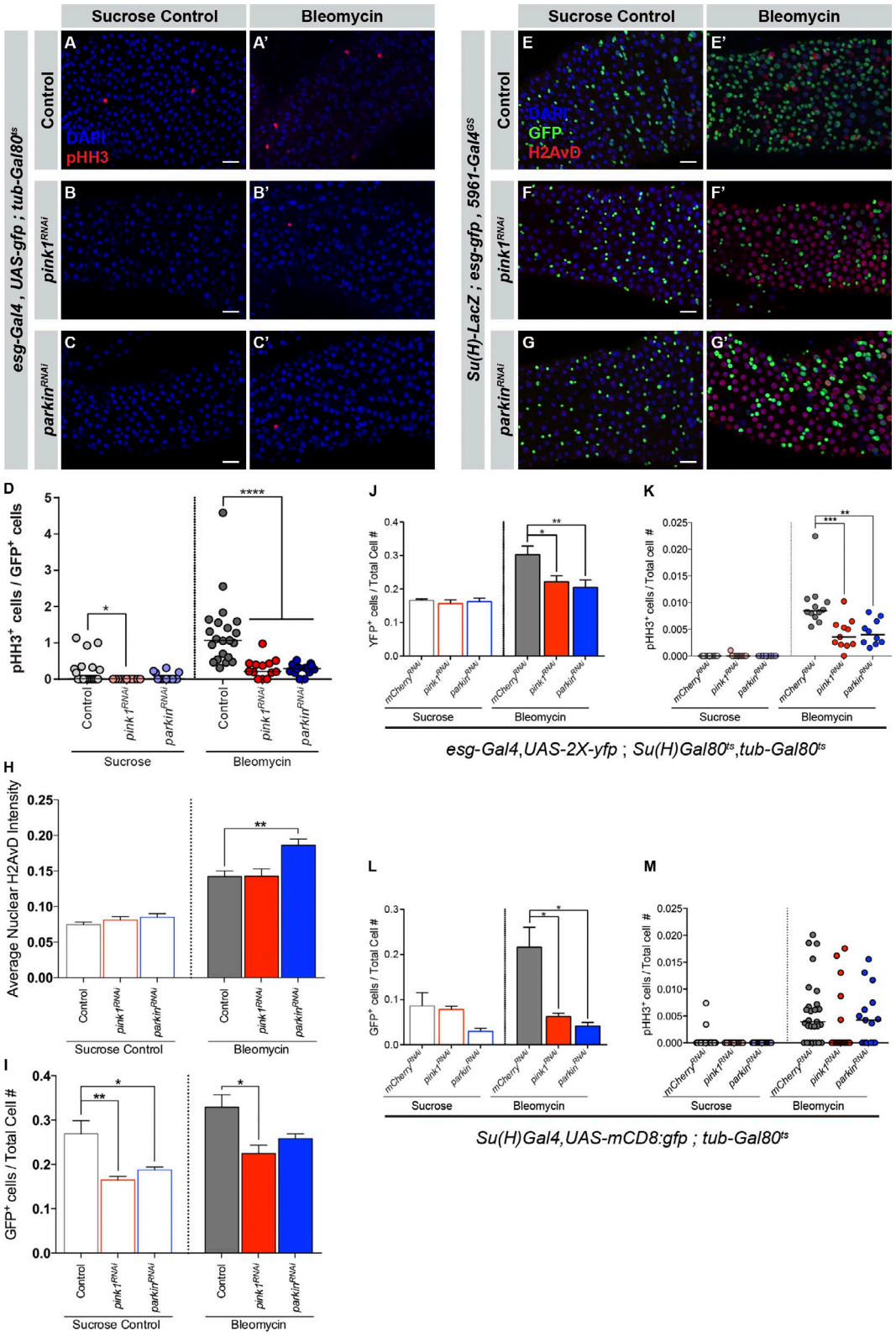

Figure 3. **Progenitor-specific depletion of Pink1 or Parkin limits the normal proliferative response to stress in the young midgut.** (A–C′) Representative immunofluorescence images of the posterior midgut of 10-d-old flies treated for 48 h with sucrose control (5% sucrose) or bleomycin (5 µg/ml in 5% sucrose) at 29°C. Bars, 20 µm. (D) Quantification of mitotic cells in the posterior midgut of flies from A–C′ in response to bleomycin-induced stress (n_{guts} = 20, 21, 14, 14, 11, and 13). Significance determined via Kruskal–Wallis test with a Dunn's post test for multiple comparisons. (E–G′) Immunofluorescence images of the posterior midgut of 10-d-old flies housed at 25°C on standard cornmeal/molasses medium supplemented with 25 µg/ml RU486 to induce transgene expression before 48 h exposure to either sucrose control (5% sucrose) or bleomycin (5 µg/ml bleomycin in 5% sucrose) medium. Bars, 20 µm. (H) Quantification of H2AvD stain intensity in the nuclei of GFP-negative cells from E–G′. (I) Quantification of *esg-gfp* reporter activity in the posterior midgut of flies from E–G′. For H and I, n_{guts} = 31, 22, 23, 32, 23, and 21. Each group of conditions represents means ± SEM and was analyzed independently

ISC proliferation in young flies as a result of other stimuli. To test for any proliferative defects upon Pink1/Parkin loss in the young gut, we induced a stress response by feeding the flies the DNA-damaging agent bleomycin. When fed to flies, bleomycin induces an increase in ISC division without affecting the fate of the progeny (Amcheslavsky et al., 2009). We used the *esg^{ts}* driver to selectively deplete Pink1 or Parkin in the progenitor cells of the gut for 7 d before bleomycin feeding. Under homeostatic conditions, the *Drosophila* midgut is largely quiescent; evidence of proliferation via pHH3 staining is elusive in young (7 d old) male midguts (Fig. 2 F). In bleomycin-fed controls, a significant increase in ISC proliferation was observed (Fig. 3, A, A′, and D). However, the increase in ISC proliferation in response to chemically induced damage was significantly attenuated upon knockdown of either Pink1 or Parkin (Fig. 3, B, B′, C, C′, and D), indicating that depletion of Pink1 or Parkin was sufficient to block ISC proliferation in response to age and damage. Similar results were obtained using *5961^{GS}* to drive expression of additional *UAS-pink1RNAi* and *UAS-parkinRNAi* lines (Fig. S3 G). We confirmed that bleomycin caused similar levels of DNA damage across the treatment groups by staining for phospho–histone 2A variant D (H2AvD), a histone variant that accumulates in response to DNA damage (Clarkson et al., 1999; Amcheslavsky et al., 2009), in flies expressing RNAi transgenes in ISCs/EBs for 10 d before bleomycin feeding. Nuclear intensity of H2AvD in ECs increased dramatically upon bleomycin feeding (Fig. 3, E–G′ and H) in all samples, indicating significant damage across genotypes.

Knockdown of Pink1, but not Parkin, also significantly inhibited the stress-induced expansion of the *esg-gfp* reporter, although Parkin knockdown samples showed a strong trend for reduced *esg-gfp* expansion (Fig. 3 I). The effect of Pink1/Parkin depletion on stress-induced expansion of *esg*$^+$ cells was further confirmed using several additional RNAi lines against Pink1 and Parkin, all of which demonstrated either a significant reduction or downward trend in expansion of *esg* (Fig. S3 H). We speculated that the increased severity of the DNA damage in Parkin-depleted samples (Fig. 3 H) resulted in an elevated stress stimulus, thus overcoming the proliferative inhibition of the ISCs. Importantly, in uninduced controls in which *5961^{GS}* is not active, neither the UAS-*pink1^{RNAi}* nor UAS-*parkin^{RNAi}* transgene limited expansion of *esg-gfp* reporter expression or demonstrated an increase in H2AvD intensity upon bleomycin feeding when compared with controls (Fig. S3, I and J, right). Interestingly, despite attenuating the ISC response to EC damage, there is no reduction in survivorship compared with controls when Pink1 or Parkin knockdown flies were aged in vials supplemented with bleomycin (Fig. S3, D–F). We previously reported that flies lacking ISCs did not demonstrate decreased survival under control conditions; however, these flies had decreased rates of survival in response to bleomycin exposure (Resende et al., 2017). Collectively, these data indicate that limited renewal of the midgut epithelium is sufficient to avoid premature death, but ISC/EB ablation can sensitize the animals to chemically induced damage.

As the age-associated increase in ISC proliferation was suppressed upon ISC- or EB-specific knockdown of Pink1 or Parkin (Fig. 2, G–J), we wanted to determine if cell type specific knockdown had similar results in young flies fed bleomycin. We once again used ISC-Gal4 and EB-Gal4 drivers to deplete Pink1 or Parkin in the ISCs or EBs, respectively. ISC-specific loss of Pink1 or Parkin inhibited the bleomycin-induced increase in ISC numbers and inhibited the increase in the number of pHH3$^+$ cells (Fig. 3, J and K; and Fig. S3, K–M and K′–M′). Alternatively, EB-specific knockdown of Pink1 or Parkin limited the expansion of EBs caused by bleomycin feeding but did not inhibit ISC proliferation (Fig. 3, L and M; and Fig. S3, N–P and N′–P′), as expected. Therefore, EB-specific knockdown affected ISC proliferation differently in aged versus bleomycin-stressed midguts (compare Fig. 2 J with Fig. 3 M). This discrepancy may be caused by the EC-specific damage caused by bleomycin, which results in elevated Upd3 signaling from the damaged ECs to ISCs that still express Pink1 and Parkin.

Pink1 or Parkin depletion results in elevated ROS in the intestinal progenitor cells of the young or aged midgut

Because Pink1 and Parkin function is critical for the identification and elimination of depolarized mitochondria, loss-of-function mutations in either gene can result in increased production of reactive oxygen species (ROS; Abramov et al., 2011). To determine whether depletion of Pink1/Parkin in the intestinal progenitors has a functional effect on the mitochondrial network, we assayed endogenous ROS production in the midgut upon ISC/EB–specific knockdown of Pink1 or Parkin. As an indirect measure for ROS production, we used a GFP reporter for the antioxidant gene *gstD1* (Sykiotis and Bohmann, 2008). In young flies with relatively quiescent ISCs, we found that *gstD1* reporter expression in ISC/EBs was lower than the surrounding ECs (Fig. 4, A–A′′). Upon knockdown of either Pink1 or Parkin, the expression of *gstD1* is elevated in the ISCs/EBs, when compared with controls (Fig. 4, B–B′′ and C–C′′). To account for variations between immunofluorescent stains, we quantified the ratio of GFP signal within progenitor cells versus the ECs immediately adjacent to the ISCs/EBs (Fig. 4 D).

A previous study demonstrated that the shift from a quiescent ISC to a proliferative state upon aging or exposure to mitogenic conditions is due, in part, to inactivation of Nrf2/CncC, a master regulator of cellular redox state (Hochmuth et al., 2011). Interestingly, our data indicate that despite increased ROS levels in the ISCs of Pink1/Parkin knockdown samples, the stem cells do not proliferate. This suggests that loss of Pink1/Parkin in midgut progenitor cells inhibits proliferation despite displaying an intrinsic pro-proliferative phenotype.

To determine if the changes to ROS levels persisted when ISCs divide more rapidly, we used live imaging of aged

with one-way ANOVA followed by Dunnett's post test. (J and K) Quantification of the proportion of ISCs in the posterior midgut (J) or mitotic ISCs (K) upon ISC-specific knockdown of mCherry, Pink1, or Parkin in 10-d-old flies treated with bleomycin (n_{guts} = 11, 11, 10, 12, 11, and 10). (L and M) Quantification of the proportion of EBs in the posterior midgut (L) or mitotic ISCs (M) upon EB-specific knockdown of mCherry, Pink1, or Parkin in flies stimulated with bleomycin at 10 d of age (n_{guts} = 24, 11, 15, 27, 16, and 15). Datasets J and L represent means ± SEM and were analyzed using one-way ANOVA followed by a Dunnett's post test to determine significant differences in means. For datasets K and M, sucrose control versus bleomycin groups were analyzed independently using a Kruskal–Wallis test for nonparametric data followed by a Dunn's post test for multiple comparisons to determine significantly different median values. *, P < 0.05; **, P < 0.01; ***, P < 0.001.

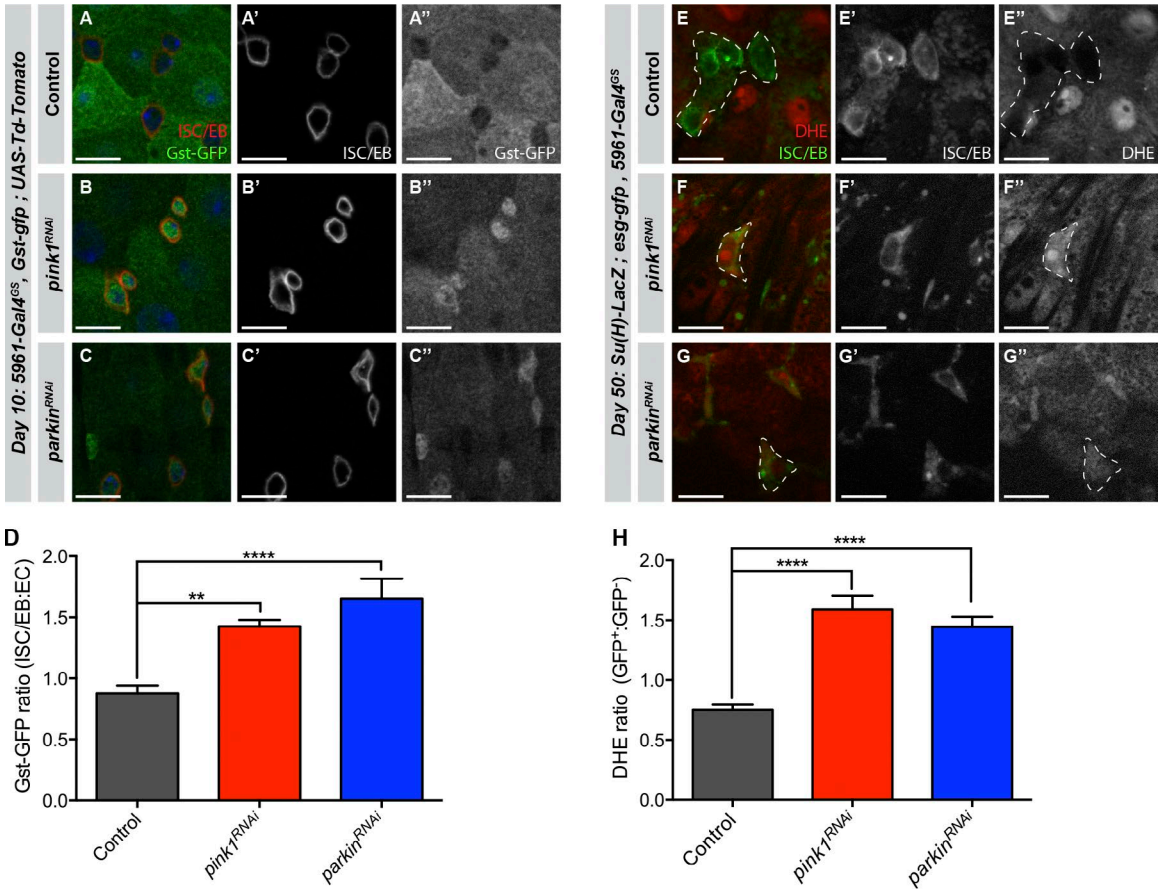

Figure 4. **Pink1 or Parkin depletion results in elevated ROS in the intestinal progenitor cells of the young or aged midgut.** (A–C′′) Representative immunofluorescence images of the posterior midguts of 10-d-old flies bearing a GstD-GFP reporter construct. Expression of *UAS-Td-Tomato* along with *mCherry*^{RNAi} (A; control), *pink1*^{RNAi} (B) or *parkin*^{RNAi} (C) was accomplished with the *5961-Gal4*^{GS} driver. *Gal4*^{GS} activity was stimulated by supplementing 25 µg/ml RU486 throughout adulthood. (D) Quantification of GstD:GFP signal from A–C reported as a ratio of GFP within the boundary of the ISCs/EBs versus the adjacent ECs (n_{guts} = 12, 11, and 11). Data are means ± SEM. (E–G′′) Example images from live-mounted posterior midguts stained with DHE from 50-d-old flies. RNAi construct expression was induced by feeding 25 µg/ml RU486 throughout adulthood to flies carrying the *5961-Gal4*^{GS} driver and *mCherry*^{RNAi} (E; control), *pink1*^{RNAi} (F), or *parkin*^{RNAi} (G). Dotted lines mark ISCs/EBs as indicated by *esg-gfp* reporter expression (E′–G′). Bars, 10 µm. (H) Quantification of the ratio of DHE within the ISCs/EBs to adjacent ECs. Data are means ± SEM. A total of 10 ISC/EB:EC comparisons were made for each gut ($n_{ISC/EB:EC\ comparisons}$ = 60, 30, and 50). Datasets were analyzed by one-way ANOVA and a Dunnett's post test. **, P < 0.01; ****, P < 0.0001.

guts (50 d old) stained with dihydroethidium (DHE), a dye whose fluorescence intensity increases upon oxidation. Similar to the *gstD1* reporter expression in the young guts, we find that ROS levels were lower in cells positive for *esg* (Fig. 4, E–E′′ and H). In contrast, ISC/EBs depleted of Pink1 or Parkin exhibited elevated levels of ROS, when compared with the surrounding ECs (Fig. 4, F–G′′ and H). These data indicate that the functional effect of loss of the mitophagic machinery exhibits effects as early as day 10 and persists throughout the life of the fly, resulting in elevated ROS levels in the progenitor cells throughout life.

Progenitor-specific depletion of Pink1/Parkin results in up-regulation of senescence-associated markers and continued proliferation defects after RNAi repression

In mammals, oncogene expression can lead to cellular senescence via increased ROS levels (Lee et al., 1999). That invertebrates also demonstrate a ROS-dependent cellular senescence phenotype has only recently been revealed. In the *Drosophila* imaginal epithelium, compromised mitochondrial function in conjunction with oncogenic Ras expression can lead to cellular senescence (Nakamura et al., 2014). Because we observed increased ROS levels in the ISCs/EBs of young and aged flies and a decrease in ISC proliferation, we investigated the possibility that ISCs depleted of Pink1 or Parkin adopt a senescence-like phenotype and, therefore, are incapable of dividing. We first tested the midguts for markers of cellular senescence, such as senescence-associated β-galactosidase (SA–β-gal) and HP-1 (Nakamura et al., 2014). Knockdown of Pink1 or Parkin, mediated by the *esgGAL4* driver, caused elevated SA–β-gal activity in many of the diploid cells of the posterior midgut (Fig. 5, A–C′). Elevated SA-β-gal levels remained even after 7 d of recovery from RNAi-induced knockdown (Fig. 5, D–D′′′). Furthermore, Pink1/Parkin depletion resulted in elevated HP-1 levels in the *esg*$^{+}$ cells of the posterior midgut (Fig. 5, E–H, arrows indicate *esg*$^{+}$ cells, ISCs, and EBs, whereas asterisks indicate polyploid, *esg*$^{-}$ cells, and ECs). HP1 levels remained unchanged in the differentiated cells of the midgut (Fig. 5 I). An additional marker of senescence, H3K9 trimethylation, was also elevated upon

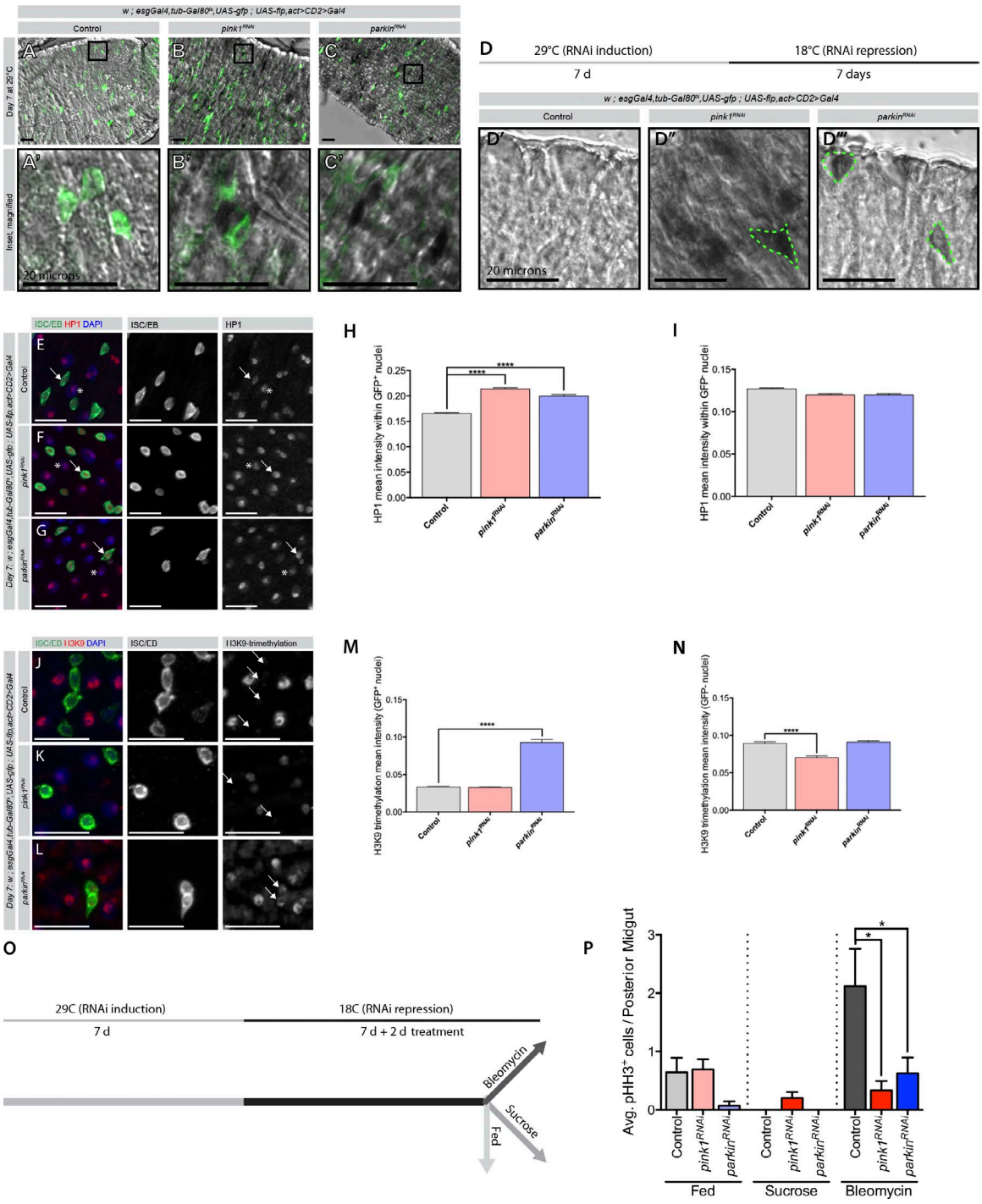

Figure 5. **Progenitor-specific depletion of Pink1/Parkin results in up-regulation of senescence-associated markers and continued proliferation defects after RNAi repression.** (A–C′) Representative senescence-associated β-galactosidase (SA-βgal) activity in the P3/P4 region of the posterior midgut. SA-βgal activity was imaged via differential interference contrast, and ISCs/EBs are shown in green via visualization of endogenous *esg-Gal4>UAS-gfp* Progenitor-specific knockdown of Pink1 (B) or Parkin (C) results in the appearance of SA-βgal activity in the posterior midgut with strong expression in some of the small, diploid, esgGFP+ cells (B′ and C′). (D) Schematic of experimental design to determine if senescence-associated markers remain after repression of RNAi expression. (D′–D‴) SA-βgal activity assays from midguts after 7 d of RNAi expression followed by 7 d of recovery (regular gene expression). (E–G) Example immunofluorescent images showing HP1 stain in the posterior midgut of 7-d-old flies upon expression of *mCherry*^{RNAi} (E; control), *pink1*^{RNAi} (F), or *parkin*^{RNAi} (G). Arrows denote ISC nuclei, and asterisks mark the nuclei of differentiated midgut cells. Bars, 20 µm. Quantification (from E–G) of mean nuclear HP1 intensity is shown for GFP+ (H; $n_{guts/cells}$ = 14/843, 13/879, and 6/374) or GFP− (I) cells ($n_{guts/cells}$ = 14/2,320, 13/2,509, and 6/2,509). (J–L) Example immunofluorescent images from the posterior midgut of 7-d-old flies showing H3K9-trimethylation up-regulation in the nuclei of ISCs/EBs depleted of Parkin. Arrows indicate nuclei of GFP-positive cells. Bars, 20 µm. (M and N) Quantification (from J–L) of GFP+ cells (M; $n_{guts/cells}$ = 11/350, 10/348, and 6/210) and GFP− cells (N; $n_{guts/cells}$ = 11/1,280, 10/1,036, 6/1,335). (O) Model of experimental design to test functional senescence upon recovery from Pink1 or Parkin depletion in the midgut progenitor cells. (P) Quantification of the number of actively dividing cells in the posterior midgut as outlined by the experiment in O (n_{guts} = 14, 13, 14, 16, 15, 14, 17, 15, and 16). H, I, M, and N were analyzed via one-way ANOVA followed by Dunnett's post tests. P was analyzed using a Kruskal–Wallis test followed by Dunn's multiple comparisons test. *, P < 0.05; ****, P < 0.0001. All graphs represent means ± SEM.

progenitor-specific knockdown of Parkin (Fig. 5, J–N). These data indicate that several hallmarks of cellular senescence are elevated in the intestinal progenitor cells in response to knockdown of Pink1/Parkin in ISCs/EBs.

Because knockdown of Pink1 or Parkin resulted in proliferative defects in the ISCs and several senescence-associated markers were expressed in ISCs upon Pink1/Parkin depletion, we next sought to determine if the ISCs are truly senescent upon ISC/EB–specific knockdown of Pink1 or Parkin and unable to reenter the cell cycle. To test for functional senescence, we used the temperature-inducible *esg* F/O approach described prevously (Fig. 2; Jiang et al., 2009). The esg F/O flies were crossed to *UAS-mCherry^{RNAi}* (control), *UAS-pink1^{RNAi}*, or *UAS-parkin^{RNAi}* at 18°C to repress RNAi expression during development. Upon eclosion, adult flies were moved to 29°C to induce expression of the RNAi constructs for 7 d. After 7 d of knockdown, the flies were returned to 18°C to once again repress the RNAi expression and allow ISCs/EBs to recover for another 7 d. At this point, flies were assayed for gut proliferation (fed samples), fed 5% sucrose for 48 h (sucrose), or fed 5 µg/ml bleomycin in 5% sucrose for 48 h (bleomycin) to stimulate ISC division (Fig. 5 O). All samples in the fed and sucrose conditions showed very little or no ISC proliferation (Fig. 5 P, left and middle). Interestingly, however, midguts that had been pulsed with *pink1^{RNAi}* or *parkin^{RNAi}* in ISCs/EBs had significantly fewer dividing ISCs upon bleomycin feeding when compared with controls (Fig. 5 P, right). These data indicate that the proliferative defect in ISCs upon Pink1 or Parkin depletion is largely irreversible. When taken together with the expression of several senescence-associated factors upon Pink1/Parkin knockdown, our data indicate that loss of Pink1 or Parkin in midgut progenitor cells results in a state resembling cellular senescence.

Cellular senescence is a potent tumor-suppressive mechanism, yet numerous recent studies have indicated that the presence of senescent cells can contribute to age-related tissue degeneration through the induction of a senescence-associated secretory phenotype (Coppé et al., 2008) and elevated levels of ROS (Passos et al., 2010). Here, we demonstrate that a block in mitochondrial turnover via depletion of Pink1 and Parkin results in hallmarks of senescence in *Drosophila* ISCs. Specifically, we show that ISC/EB–specific reduction of Pink1 and Parkin leads to significant intracellular damage and alterations to mitochondrial morphology (Fig. 1 and Fig. S1, L–P). These changes in mitochondrial ultrastructure correlate with a block in the uncontrolled ISC proliferation normally present in aged animals and induced in response to acute intestinal damage (Figs. 2 and 3; Fig. S2, E–H′′; and Fig. S3, G–P′). The block in ISC proliferation is observed in the presence of high levels of ROS in Pink1- and Parkin-depleted ISCs (Fig. 4), which would normally stimulate ISC division. Lastly, we show that several hallmarks of senescence are elevated in ISCs upon depletion of Pink1 or Parkin and that ISCs appear to be functionally senescent, as stress-induced proliferation remains limited even after RNAi repression is relieved (Fig. 5). Collectively, our results indicate that progenitor-specific mitochondrial dysfunction uncouples cellular and tissue aging, in part, through induction of ISC senescence and suggest that ISCs use mitophagy as one strategy to maintain a healthy complement of mitochondria. The role of mitochondria in enhancing the onset of senescence has been recently reported in mammals (Correia-Melo et al., 2016), and our data reveal that a similar relationship is present in invertebrates.

Materials and methods

Fly food and husbandry

Flies were cultured in vials containing standard cornmeal medium (in wt/vol, 1% agar, 3% brewer's yeast, 1.9% sucrose, 3.8% dextrose, and 9.1% cornmeal). Flies carrying the drug-inducible Gal4/UAS system, GeneSwitch (Osterwalder et al., 2001; Roman et al., 2001), were cultured at 25°C; transgene induction was performed by supplementing the food with 25 µg/ml of the steroid hormone mifepristone (RU486, M8046; Sigma-Aldrich). Flies carrying the temperature-inducible Gal4/UAS system, TARGET (McGuire et al., 2004), were crossed at 18°C to repress transgene expression. Upon eclosion, flies were cultured at 29°C to induce Gal4-dependent expression. In all cases, flies were flipped to fresh media every 2 or 3 d. Male flies were used in all assays described.

RNAi screen for mitochondria-related genes affecting tissue homeostasis and ISC proliferation

The following transgenic lines were used in this assay: *UAS-dPGC-1* (Rera et al., 2011), *UAS-dPGC-1^{RNAi}* and *UAS-drp:HA* (obtained from D.W. Walker, University of California, Los Angeles, Los Angeles, CA), *UAS-drp^{RNAi}* (FBst0027682), *UAS-Opa1^{RNAi}* (FBst0032358), *UAS-marf^{RNAi}* (FBst0031157), *UAS-tamas^{RNAi}* (FBst0031098), *UAS-milton^{RNAi}* (FBst0028385), *UAS-miro^{RNAi}* (FBst0027659), *UAS-RalA^{RNAi}* (FBst0029580), *UAS-Pink1^{RNAi}* (FBst0031170), and *UAS-Parkin^{RNAi}* (FBst0037509). These transgenic lines were crossed to *5961-Gal4^{GS}/UAS-gfp^{mito}* flies, and the progeny were aged at 25°C for 10, 30, or 50 d. Tissue homeostasis was assayed by tissue morphology, GFP expression, ISC proliferation, and mitochondrial morphology.

Drosophila strains

The following TRiP (Transgenic RNAi Project, Harvard Medical School) RNAi lines were obtained from the Bloomington Stock Center: *UAS-Pink1^{RNAi}* (BL#31170, FBst0031170), *UAS-Pink1^{RNAi}* (BL#31262, FBst0031262), *UAS-Pink1^{RNAi}* (BL#38262, FBst0038262), *UAS-Parkin^{RNAi}* (BL#31259, FBst0031259), *UAS-Parkin^{RNAi}* (37509, FBst0037509), *UAS-Luciferase^{RNAi}* (BL#31603, FBst0031603), and *UAS-mCherry^{RNAi}* (BL#35785, FBst0035785). An additional *UAS-Parkin^{RNAi}* line was obtained from the Vienna Drosophila Resource Center (v104363, FBst0476221). RU486-inducible *5961^{GS}* (FBti0150383) and *5966^{GS}* (FBti0150384) drivers were described previously (Nicholson et al., 2008) and provided by H. Jasper (Buck Institute for Research on Aging, Novato, CA). The *esg-GFP* enhancer trap line (P01986, FBtp0051138) was obtained from L. Cooley (Yale School of Medicine, New Haven, CT) as part of the FlyTrap collection. The reporter lines *UAS-GFP^{mito}* (BL#8443, FBst0008443) and *UAS-LacZ^{nls}* (BL#3956, FBst0003956) were acquired from Bloomington. *w;esg-Gal4,UAS-GFP,tubGal80^{TS}/CyO; UAS-flp,act>CD2>Gal4/Tm6b* (*escargot* F/O) line was obtained from B. Edgar (Huntsman Cancer Institute, Salt Lake City, UT). *Su(H)Gal4,*UAS-*GFP^{CD8}/CyO;tubGal80^{TS}/MKRS* (EB-Gal4) and *esgGal4,UAS-2xYFP/CyO;Su(H)Gal80, tubGal80^{TS}/TM3, Sb* (ISC-Gal4) were gifts from S. Hou (Center for Cancer Research, National Cancer Institute, Frederick, MD). *Da-Gal^{GeneSwitch}* was obtained from D.W. Walker. The *UAS-roGFP^{Mito}* was a gift from R. Demarco (University of California, Los Angeles, Los Angeles, CA).

Bleomycin feeding experiments

For experiments with Gal80^{ts}-dependent induction, flies were collected 1 or 2 d after eclosion and shifted to 29°C on standard cornmeal/molasses medium for 7 d before being transferred to treatment vials. In experiments with GeneSwitch-based induction, flies were collected 1 or 2 d after eclosion and reared on standard medium for 10 d at 25°C before

being transferred to treatment vials. Treatment vials consisted of empty vials containing a folded KimWipe saturated with 750 µl of uninduced control (0.25% vol/vol ethanol in 5% sucrose), induced control (25 µg/ml RU486 in 5% sucrose), uninduced treatment (0.25% vol/vol ethanol and 5 µg/ml bleomycin in 5% sucrose), and induced treatment (25 µg/ml RU486 and 5 µg/ml bleomycin in 5% sucrose).

Survivorship

All progeny from parental crosses were collected within 24 h of eclosion and allowed to mate for 2 d before sorting for the appropriate genotypes using light CO_2 anesthesia. Flies were housed in a 25°C incubator kept on a 12 h light/dark cycle. For standard life span experiments, the flies were housed at a density of 20 flies per vial and flipped to new vials with standard cornmeal/molasses medium containing either ethanol (0.25% vol/vol as vehicle for uninduced GeneSwitch controls) or 25 µg/ml RU486 every 2 or 3 d. For bleomycin survivorship experiments, flies were collected as before but aged to 10 d on standard food containing either 25 µg/ml RU486 or 0.25% vol/vol ethanol before being transferred to treatment vials described in the previous section.

Immunostaining and microscopy

The *Drosophila* gastrointestinal tract was dissected into 4% paraformaldehyde in PLP buffer and fixed for 1 h at room temperature. The tissue washes were performed with PBT (1× PBS and 0.1% Triton X-100). Antibody incubations were performed in PBT supplemented with 3% BSA and 0.02% sodium azide. Primary antibodies incubated at room temperature for at least 4 h or overnight at 4°C; secondary antibody incubations were 2 h at room temperature. Fixed and stained tissue was whole mounted in Vectashield mounting medium containing DAPI from Vector Laboratories. Primary antibodies used in this study included mouse α-FK2 (polyubiquitin; 1:200; Enzo Life Sciences), rabbit α-GFP (1:5,000; A11122; Molecular Probes), mouse α-GFP (1:200; A11120; Molecular Probes), chicken α-GFP (1:1,000; Aves Labs Inc.), rabbit α-βGal (1:2,000; Cappel), rabbit α(phospho–histone-H3 (1:200; 06–570; EMD Millipore), rabbit α-H2AvD pS137 (1:200; 600–401-914; Rockland), and mouse α-βGal (1:20; 40-1a), mouse α-Armadillo (1:20; N2 7A1), mouse α-HP1 (C1A9), and mouse α-Prospero (1:100; MR1A; Developmental Studies Hybridoma Bank).

Superresolution images were obtained from a custom-build STED superresolution microscope currently reaching a resolution of ∼30 to 40 nm.

Image analysis

For quantification of ISCs/EBs, clone number and size, H2AvD intensity, or pHH3 in the posterior midgut, images were acquired at room temperature using a 40× objective on either a ZEISS LSM 780 confocal microscope running Zen software (ZEISS) or an Axio Observer.Z1 (ZEISS) fitted with an ApoTome running AxioVision software. To image the entire posterior midgut, three to five images were taken to cover the area from the pylorus to the posterior aspect of the iron/copper region, corresponding to the P3 to P4 region of the *Drosophila* midgut (Marianes and Spradling, 2013). Each image was acquired as a three-plane Z-stack spaced at 0.75 µm. Raw images were converted to max intensity projections using ImageJ. Image features were quantified with custom CellProfiler pipelines.

EM

The gastrointestinal tract was dissected into 2% EM-grade glutaraldehyde in PBS and fixed for 1 h at room temperature and then 2 h on ice. Samples were washed in PBS before embedding in soft agar. Tissues underwent secondary fixation in 1% osmium tetroxide plus 0.3% potassium ferricyanide. Guts were then en bloc stained with 2% uranyl acetate, dehydrated in ethanol, and embedded in EPON epoxy resin. For standard TEM, thin sections were mounted on slot grids and stained with uranyl acetate and lead citrate. Images were acquired using a Libra 120 PLUS EF-TEM transmission electron microscope (ZEISS) or a 100CX transmission electron microscope (JEOL). For tomographic studies, both sides of semi-thick sections were coated with gold particles and tilt series collected using an FEI Titan 80–300 (CTWIN) IVEM/STEM. Tomographic reconstructions and 3D models of mitochondria were generated with IMOD and TxBR.

Senescence-associated β-galactosidase assay

Full, intact midguts were stained for senescent cells using the Senescence Cells Histochemical Staining kit (CS0030; Sigma-Aldrich). In brief, 10-d-old flies were anesthetized by covering the culture vial with ice until the flies fell to the bottom of the vial. Flies were immediately dissected into 1× PBS. Dissection of flies from all of the genotypes to be analyzed would take place in a 15-min window, after which the remainder of the staining protocol would be performed as follows. Guts were washed twice with 1× PBS before being lightly fixed for 5 min at room temperature in 1× fixation buffer. Guts were washed three times in 1× PBS before being incubated in 1× staining mixture (mixed as per kit instructions) at 37°C for 30 min. After staining, the midguts were washed in 1× PBS and mounted in 1× PBS on Superfrost Plus micro slides (VWR 48311–703). The guts were images immediately on an Axio Imager A2 microscope (ZEISS) using Zen imaging software or an Axio Observer.Z1 fitted with an ApoTome.

Statistical analysis

When datasets followed a normal distribution, significance was determined via one-way ANOVA followed by a Dunnett's multiple comparison test. When data were nonnormally distributed (typically pHH3 count data), a nonparametric Kruskal–Wallis analysis was used followed by a Dunn's multiple comparison test. Any deviations from this standard are noted in the text.

Online supplemental material

Fig. S1 contains data demonstrating the effect of ubiquitous Pink1 or Parkin knockdown on mitochondrial morphology in the flight muscle, wing posture, and climbing ability. These phenotypes are similar to those observed in Pink1 and Parkin mutants, which provides evidence for the efficacy of the Pink1 and Parkin constructs in vivo. Furthermore, quantification of the frequency of progenitor cell mitochondrial abnormalities (as observed by TEM) upon progenitor-specific knockdown of Pink1 or Parkin is provided. Fig. S2 demonstrates the cell-specific nature of the observed phenotypes upon Pink1 or Parkin knockdown and indicates that the phenotypes are not caused by perdurance of the RNAi construct into the differentiated ECs. In addition, representative immunofluorescent images from progenitor-, ISC-, and EB-specific knockdown of Pink1 or Parkin are included. Fig. S3 contains lifespan and survivorship data that shows progenitor-specific knockdown of Pink1 or Parkin does not affect lifespan or survivorship under bleomycin-induced stress. Despite having no effect on survivorship, several additional Pink1 and Parkin RNAi lines were analyzed as redundant controls; these lines also limited the stress-induced proliferative response of ISCs. Lastly, representative immunofluorescent images of bleomycin-stressed guts from ISC- or EB-specific Pink1 or Parkin knockdown samples are included.

Acknowledgments

We thank Drs. H. Jasper, B. Edgar, L. Cooley, S. Hou, the Bloomington Stock Center, the Vienna Drosophila Resource Center, and the TRiP at

Harvard Medical School (National Institutes of Health/National Institute of General Medical Sciences R01-GM084947) for providing transgenic RNAi fly stocks and/or plasmid vectors used in this study and Dr. D. Walker and the Jones laboratory for helpful discussions. In addition, we thank Dr. Yong Wu and Dr. Enrico Stefani for the use of their custom STED microscope. The STED system was built in the Department of Anesthesiology, University of California, Los Angeles, supported by a National Institutes of Health grant from the National Heart, Lung, and Blood Institute (BRG R01 HL088640).

This work was supported by the Eli and Edythe Broad Center of Regenerative Medicine and Stem Cell Research at the University of California, Los Angeles (D.L. Jones), the National Institutes of Health (grants AG028092, AG040288, and AG052732 to D.L. Jones and grant 5P41GM103412-28 to M.H. Ellisman), and the National Science Foundation (graduate research fellowship DGE-1144087 to C.L. Koehler).

The authors declare no competing financial interests.

Author contributions: Conceptualization, C.L. Koehler and D.L. Jones; Methodology, C.L. Koehler, G.A. Perkins, and D.L. Jones; Formal analysis, C.L. Koehler; Investigation, C.L. Koehler and G.A. Perkins; Resources, M.H. Ellisman; Writing of original draft, C.L. Koehler and D.L. Jones; Writing, Review, and editing, C.L. Koehler, D.L. Jones, G.A. Perkins, and M.H. Ellisman; Visualization, C.L. Koehler and D.L. Jones; Supervision, D.L. Jones; Funding Acquisition, M.H. Ellisman and D.L. Jones.

Submitted: 12 October 2016
Revised: 14 May 2017
Accepted: 15 June 2017

References

Abramov, A.Y., M. Gegg, A. Grunewald, N.W. Wood, C. Klein, and A.H. Schapira. 2011. Bioenergetic consequences of PINK1 mutations in Parkinson disease. *PLoS One.* 6:e25622. http://dx.doi.org/10.1371/journal.pone.0025622

Amcheslavsky, A., J. Jiang, and Y.T. Ip. 2009. Tissue damage-induced intestinal stem cell division in *Drosophila*. *Cell Stem Cell.* 4:49–61. http://dx.doi.org/10.1016/j.stem.2008.10.016

Amcheslavsky, A., N. Ito, J. Jiang, and Y.T. Ip. 2011. Tuberous sclerosis complex and Myc coordinate the growth and division of *Drosophila* intestinal stem cells. *J. Cell Biol.* 193:695–710. http://dx.doi.org/10.1083/jcb.201103018

Amcheslavsky, A., W. Song, Q. Li, Y. Nie, I. Bragatto, D. Ferrandon, N. Perrimon, and Y.T. Ip. 2014. Enteroendocrine cells support intestinal stem-cell-mediated homeostasis in *Drosophila*. *Cell Reports.* 9:32–39. http://dx.doi.org/10.1016/j.celrep.2014.08.052

Benard, G., and R. Rossignol. 2008. Ultrastructure of the mitochondrion and its bearing on function and bioenergetics. *Antioxid. Redox Signal.* 10:1313–1342. http://dx.doi.org/10.1089/ars.2007.2000

Biteau, B., and H. Jasper. 2011. EGF signaling regulates the proliferation of intestinal stem cells in *Drosophila*. *Development.* 138:1045–1055. http://dx.doi.org/10.1242/dev.056671

Biteau, B., and H. Jasper. 2014. Slit/Robo signaling regulates cell fate decisions in the intestinal stem cell lineage of *Drosophila*. *Cell Reports.* 7:1867–1875. http://dx.doi.org/10.1016/j.celrep.2014.05.024

Biteau, B., J. Karpac, S. Supoyo, M. Degennaro, R. Lehmann, and H. Jasper. 2010. Lifespan extension by preserving proliferative homeostasis in *Drosophila*. *PLoS Genet.* 6:e1001159. http://dx.doi.org/10.1371/journal.pgen.1001159

Buchon, N., N.A. Broderick, S. Chakrabarti, and B. Lemaitre. 2009a. Invasive and indigenous microbiota impact intestinal stem cell activity through multiple pathways in *Drosophila*. *Genes Dev.* 23:2333–2344. http://dx.doi.org/10.1101/gad.1827009

Buchon, N., N.A. Broderick, M. Poidevin, S. Pradervand, and B. Lemaitre. 2009b. *Drosophila* intestinal response to bacterial infection: Activation of host defense and stem cell proliferation. *Cell Host Microbe.* 5:200–211. http://dx.doi.org/10.1016/j.chom.2009.01.003

Buchon, N., D. Osman, F.P. David, H.Y. Fang, J.P. Boquete, B. Deplancke, and B. Lemaitre. 2013. Morphological and molecular characterization of adult midgut compartmentalization in *Drosophila*. *Cell Reports.* 3:1725–1738. http://dx.doi.org/10.1016/j.celrep.2013.04.001

Clark, I.E., M.W. Dodson, C. Jiang, J.H. Cao, J.R. Huh, J.H. Seol, S.J. Yoo, B.A. Hay, and M. Guo. 2006. *Drosophila* pink1 is required for mitochondrial function and interacts genetically with parkin. *Nature.* 441:1162–1166. http://dx.doi.org/10.1038/nature04779

Clarkson, M.J., J.R. Wells, F. Gibson, R. Saint, and D.J. Tremethick. 1999. Regions of variant histone His2AvD required for *Drosophila* development. *Nature.* 399:694–697. http://dx.doi.org/10.1038/21436

Coppé, J.P., C.K. Patil, F. Rodier, Y. Sun, D.P. Muñoz, J. Goldstein, P.S. Nelson, P.Y. Desprez, and J. Campisi. 2008. Senescence-associated secretory phenotypes reveal cell-nonautonomous functions of oncogenic RAS and the p53 tumor suppressor. *PLoS Biol.* 6:2853–2868. http://dx.doi.org/10.1371/journal.pbio.0060301

Correia-Melo, C., F.D. Marques, R. Anderson, G. Hewitt, R. Hewitt, J. Cole, B.M. Carroll, S. Miwa, J. Birch, A. Merz, et al. 2016. Mitochondria are required for pro-ageing features of the senescent phenotype. *EMBO J.* 35:724–742. http://dx.doi.org/10.15252/embj.201592862

Deng, H., M.W. Dodson, H. Huang, and M. Guo. 2008. The Parkinson's disease genes pink1 and parkin promote mitochondrial fission and/or inhibit fusion in *Drosophila*. *Proc. Natl. Acad. Sci. USA.* 105:14503–14508. http://dx.doi.org/10.1073/pnas.0803998105

Greene, J.C., A.J. Whitworth, I. Kuo, L.A. Andrews, M.B. Feany, and L.J. Pallanck. 2003. Mitochondrial pathology and apoptotic muscle degeneration in *Drosophila* parkin mutants. *Proc. Natl. Acad. Sci. USA.* 100:4078–4083. http://dx.doi.org/10.1073/pnas.0737556100

Guo, Z., and B. Ohlstein. 2015. Stem cell regulation. Bidirectional Notch signaling regulates *Drosophila* intestinal stem cell multipotency. *Science.* 350: aab0988. http://dx.doi.org/10.1126/science.aab0988

Hackenbrock, C.R. 1966. Ultrastructural bases for metabolically linked mechanical activity in mitochondria. I. Reversible ultrastructural changes with change in metabolic steady state in isolated liver mitochondria. *J. Cell Biol.* 30:269–297. http://dx.doi.org/10.1083/jcb.30.2.269

Han, H., C. Pan, C. Liu, X. Lv, X. Yang, Y. Xiong, Y. Lu, W. Wu, J. Han, Z. Zhou, et al. 2015. Gut-neuron interaction via Hh signaling regulates intestinal progenitor cell differentiation in *Drosophila*. *Cell Discov.* 1:15006. http://dx.doi.org/10.1038/celldisc.2015.6

Henchcliffe, C., and M.F. Beal. 2008. Mitochondrial biology and oxidative stress in Parkinson disease pathogenesis. *Nat. Clin. Pract. Neurol.* 4:600–609. http://dx.doi.org/10.1038/ncpneuro0924

Hochmuth, C.E., B. Biteau, D. Bohmann, and H. Jasper. 2011. Redox regulation by Keap1 and Nrf2 controls intestinal stem cell proliferation in *Drosophila*. *Cell Stem Cell.* 8:188–199. http://dx.doi.org/10.1016/j.stem.2010.12.006

Hur, J.H., S. Bahadorani, J. Graniel, C.L. Koehler, M. Ulgherait, M. Rera, D.L. Jones, and D.W. Walker. 2013. Increased longevity mediated by yeast NDI1 expression in *Drosophila* intestinal stem and progenitor cells. *Aging (Albany NY).* 5:662–681. http://dx.doi.org/10.18632/aging.100595

Jiang, H., and B.A. Edgar. 2009. EGFR signaling regulates the proliferation of *Drosophila* adult midgut progenitors. *Development.* 136:483–493. http://dx.doi.org/10.1242/dev.026955

Jiang, H., P.H. Patel, A. Kohlmaier, M.O. Grenley, D.G. McEwen, and B.A. Edgar. 2009. Cytokine/Jak/Stat signaling mediates regeneration and homeostasis in the *Drosophila* midgut. *Cell.* 137:1343–1355. http://dx.doi.org/10.1016/j.cell.2009.05.014

Jones, D.L., and T.A. Rando. 2011. Emerging models and paradigms for stem cell ageing. *Nat. Cell Biol.* 13:506–512. http://dx.doi.org/10.1038/ncb0511-506

Kashatus, D.F., K.H. Lim, D.C. Brady, N.L. Pershing, A.D. Cox, and C.M. Counter. 2011. RALA and RALBP1 regulate mitochondrial fission at mitosis. *Nat. Cell Biol.* 13:1108–1115. http://dx.doi.org/10.1038/ncb2310

Lee, W.-J. 2009. Bacterial-modulated host immunity and stem cell activation for gut homeostasis. *Genes Dev.* 23:2260–2265. http://dx.doi.org/10.1101/gad.1858709

Lee, A.C., B.E. Fenster, H. Ito, K. Takeda, N.S. Bae, T. Hirai, Z.X. Yu, V.J. Ferrans, B.H. Howard, and T. Finkel. 1999. Ras proteins induce senescence by altering the intracellular levels of reactive oxygen species. *J. Biol. Chem.* 274:7936–7940. http://dx.doi.org/10.1074/jbc.274.12.7936

Li, H., Y. Qi, and H. Jasper. 2013. Dpp signaling determines regional stem cell identity in the regenerating adult *Drosophila* gastrointestinal tract. *Cell Reports.* 4:10–18. http://dx.doi.org/10.1016/j.celrep.2013.05.040

Liu, W., S.R. Singh, and S.X. Hou. 2010. JAK-STAT is restrained by Notch to control cell proliferation of the *Drosophila* intestinal stem cells. *J. Cell. Biochem.* 109:992–999.

Maeda, K., M. Takemura, M. Umemori, and T. Adachi-Yamada. 2008. E-cadherin prolongs the moment for interaction between intestinal stem cell and its progenitor cell to ensure Notch signaling in adult *Drosophila* midgut. *Genes Cells.* 13:1219–1227. http://dx.doi.org/10.1111/j.1365-2443.2008.01239.x

Marianes, A., and A.C. Spradling. 2013. Physiological and stem cell compartmentalization within the *Drosophila* midgut. *eLife.* 2:e00886. http://dx.doi.org/10.7554/eLife.00886

McGuire, S.E., Z. Mao, and R.L. Davis. 2004. Spatiotemporal gene expression targeting with the TARGET and gene-switch systems in *Drosophila. Sci. STKE.* 2004:pl6.

Micchelli, C.A., and N. Perrimon. 2006. Evidence that stem cells reside in the adult *Drosophila* midgut epithelium. *Nature.* 439:475–479. http://dx.doi.org/10.1038/nature04371

Myant, K.B., A. Scopelliti, S. Haque, M. Vidal, O.J. Sansom, and J.B. Cordero. 2013. Rac1 drives intestinal stem cell proliferation and regeneration. *Cell Cycle.* 12:2973–2977. http://dx.doi.org/10.4161/cc.26031

Nakamura, M., S. Ohsawa, and T. Igaki. 2014. Mitochondrial defects trigger proliferation of neighbouring cells via a senescence-associated secretory phenotype in *Drosophila*. *Nat. Commun.* 5:5264. http://dx.doi.org/10.1038/ncomms6264

Nicholson, L., G.K. Singh, T. Osterwalder, G.W. Roman, R.L. Davis, and H. Keshishian. 2008. Spatial and temporal control of gene expression in *Drosophila* using the inducible GeneSwitch GAL4 system. I. Screen for larval nervous system drivers. *Genetics.* 178:215–234. http://dx.doi.org/10.1534/genetics.107.081968

O'Brien, L.E., S.S. Soliman, X. Li, and D. Bilder. 2011. Altered modes of stem cell division drive adaptive intestinal growth. *Cell.* 147:603–614. http://dx.doi.org/10.1016/j.cell.2011.08.048

Ohlstein, B., and A. Spradling. 2006. The adult *Drosophila* posterior midgut is maintained by pluripotent stem cells. *Nature.* 439:470–474. http://dx.doi.org/10.1038/nature04333

Ohlstein, B., and A. Spradling. 2007. Multipotent *Drosophila* intestinal stem cells specify daughter cell fates by differential notch signaling. *Science.* 315:988–992.

Osterwalder, T., K.S. Yoon, B.H. White, and H. Keshishian. 2001. A conditional tissue-specific transgene expression system using inducible GAL4. *Proc. Natl. Acad. Sci. USA.* 98:12596–12601. http://dx.doi.org/10.1073/pnas.221303298

Park, J., S.B. Lee, S. Lee, Y. Kim, S. Song, S. Kim, E. Bae, J. Kim, M. Shong, J.M. Kim, and J. Chung. 2006. Mitochondrial dysfunction in *Drosophila* PINK1 mutants is complemented by parkin. *Nature.* 441:1157–1161. http://dx.doi.org/10.1038/nature04788

Passos, J.F., G. Nelson, C. Wang, T. Richter, C. Simillion, C.J. Proctor, S. Miwa, S. Olijslagers, J. Hallinan, A. Wipat, et al. 2010. Feedback between p21 and reactive oxygen production is necessary for cell senescence. *Mol. Syst. Biol.* 6:347. http://dx.doi.org/10.1038/msb.2010.5

Poole, A.C., R.E. Thomas, L.A. Andrews, H.M. McBride, A.J. Whitworth, and L.J. Pallanck. 2008. The PINK1/Parkin pathway regulates mitochondrial morphology. *Proc. Natl. Acad. Sci. USA.* 105:1638–1643. http://dx.doi.org/10.1073/pnas.0709336105

Poole, A.C., R.E. Thomas, S. Yu, E.S. Vincow, and L. Pallanck. 2010. The mitochondrial fusion-promoting factor mitofusin is a substrate of the PINK1/parkin pathway. *PLoS One.* 5:e10054. http://dx.doi.org/10.1371/journal.pone.0010054

Rana, A., M. Rera, and D.W. Walker. 2013. Parkin overexpression during aging reduces proteotoxicity, alters mitochondrial dynamics, and extends lifespan. *Proc. Natl. Acad. Sci. USA.* 110:8638–8643. http://dx.doi.org/10.1073/pnas.1216197110

Rera, M., S. Bahadorani, J. Cho, C.L. Koehler, M. Ulgherait, J.H. Hur, W.S. Ansari, T. Lo Jr., D.L. Jones, and D.W. Walker. 2011. Modulation of longevity and tissue homeostasis by the *Drosophila* PGC-1 homolog. *Cell Metab.* 14:623–634. http://dx.doi.org/10.1016/j.cmet.2011.09.013

Resende, L.P., M.E. Truong, A. Gomez, and D.L. Jones. 2017. Intestinal stem cell ablation reveals differential requirements for survival in response to chemical challenge. *Dev. Biol.* 424:10–17. http://dx.doi.org/10.1016/j.ydbio.2017.01.004

Resnik-Docampo, M., C.L. Koehler, R.I. Clark, J.M. Schinaman, V. Sauer, D.M. Wong, S. Lewis, C. D'Alterio, D.W. Walker, and D.L. Jones. 2017. Tricellular junctions regulate intestinal stem cell behaviour to maintain homeostasis. *Nat. Cell Biol.* 19:52–59. http://dx.doi.org/10.1038/ncb3454

Roman, G., K. Endo, L. Zong, and R.L. Davis. 2001. P[Switch], a system for spatial and temporal control of gene expression in *Drosophila melanogaster*. *Proc. Natl. Acad. Sci. USA.* 98:12602–12607. http://dx.doi.org/10.1073/pnas.221303998

Springer, W., and P.J. Kahle. 2011. Regulation of PINK1-Parkin-mediated mitophagy. *Autophagy.* 7:266–278. http://dx.doi.org/10.4161/auto.7.3.14348

Sykiotis, G.P., and D. Bohmann. 2008. Keap1/Nrf2 signaling regulates oxidative stress tolerance and lifespan in *Drosophila*. *Dev. Cell.* 14:76–85. http://dx.doi.org/10.1016/j.devcel.2007.12.002

Takashima, S., K.L. Adams, P.A. Ortiz, C.T. Ying, R. Moridzadeh, A. Younossi-Hartenstein, and V. Hartenstein. 2011. Development of the *Drosophila* entero-endocrine lineage and its specification by the Notch signaling pathway. *Dev. Biol.* 353:161–172. http://dx.doi.org/10.1016/j.ydbio.2011.01.039

Tian, A., and J. Jiang. 2014. Intestinal epithelium-derived BMP controls stem cell self-renewal in *Drosophila* adult midgut. *eLife.* 3:e01857. http://dx.doi.org/10.7554/eLife.01857

Twig, G., A. Elorza, A.J. Molina, H. Mohamed, J.D. Wikstrom, G. Walzer, L. Stiles, S.E. Haigh, S. Katz, G. Las, et al. 2008. Fission and selective fusion govern mitochondrial segregation and elimination by autophagy. *EMBO J.* 27:433–446. http://dx.doi.org/10.1038/sj.emboj.7601963

Wang, L., C.J. McLeod, and D.L. Jones. 2011. Regulation of adult stem cell behavior by nutrient signaling. *Cell Cycle.* 10:2628–2634. http://dx.doi.org/10.4161/cc.10.16.17059

Wang, L., X. Zeng, H.D. Ryoo, and H. Jasper. 2014. Integration of UPR ER and oxidative stress signaling in the control of intestinal stem cell proliferation. *PLoS Genet.* 10:e1004568. http://dx.doi.org/10.1371/journal.pgen.1004568

Wei, H., L. Liu, and Q. Chen. 2015. Selective removal of mitochondria via mitophagy: distinct pathways for different mitochondrial stresses. *Biochim. Biophys. Acta.* 1853(10 Pt B):2784–2790. http://dx.doi.org/10.1016/j.bbamcr.2015.03.013

Westermann, B. 2012. Bioenergetic role of mitochondrial fusion and fission. *Biochim. Biophys. Acta.* 1817:1833–1838. http://dx.doi.org/10.1016/j.bbabio.2012.02.033

Yang, Y., Y. Ouyang, L. Yang, M.F. Beal, A. McQuibban, H. Vogel, and B. Lu. 2008. Pink1 regulates mitochondrial dynamics through interaction with the fission/fusion machinery. *Proc. Natl. Acad. Sci. USA.* 105:7070–7075. http://dx.doi.org/10.1073/pnas.0711845105

Youle, R.J., and D.P. Narendra. 2011. Mechanisms of mitophagy. *Nat. Rev. Mol. Cell Biol.* 12:9–14. http://dx.doi.org/10.1038/nrm3028

Zeng, X., and S.X. Hou. 2015. Enteroendocrine cells are generated from stem cells through a distinct progenitor in the adult *Drosophila* posterior midgut. *Development.* 142:644–653. http://dx.doi.org/10.1242/dev.113357

Zeng, X., C. Chauhan, and S.X. Hou. 2010. Characterization of midgut stem cell- and enteroblast-specific Gal4 lines in *Drosophila. Genesis.* 48:607–611.

Zhu, J., K.Z. Wang, and C.T. Chu. 2013. After the banquet: Mitochondrial biogenesis, mitophagy, and cell survival. *Autophagy.* 9:1663–1676. http://dx.doi.org/10.4161/auto.24135